Journal of Controlled Release 380 (2025) 396–403

Contents lists available at ScienceDirect

Journal of Controlled Release

journal homepage: www.elsevier.com/locate/jconrel

The strategy used by naïve anti-PEG antibodies to capture flexible and featureless PEG chains

Yiwei Liu [a,1,2], Takahiro Mori [b,1], Yusei Ito [c,1], Kimiko Kuroki [d,1], Seiichiro Hayashi [e], Daisuke Kohda [e], Taro Shimizu [f], Tatsuhiro Ishida [f], Steve R. Roffler [g,h], Mika K. Kaneko [i], Yukinari Kato [i], Takao Arimori [j], Takamasa Teramoto [b], Kazuhiro Takemura [c,k], Kenta Ishibashi [a], Yoshiki Katayama [a], Katsumi Maenaka [d,*], Yoshimitsu Kakuta [b,*], Akio Kitao [c,*], Takeshi Mori [a,*]

[a] Department of Applied Chemistry, Faculty of Engineering, Kyushu University, 744 Motooka, Nishi-ku, Fukuoka 819-0395, Japan
[b] Department of Bioscience and Biotechnology, Faculty of Agriculture, Kyushu University, 744 Motooka, Nishi-ku, Fukuoka 819-0395, Japan
[c] School of Life Science and Technology, Institute of Science Tokyo, 2-12-1 Ookayama, Meguro, Tokyo 152-8550, Japan
[d] Laboratory of Biomolecular Science, Faculty of Pharmaceutical Sciences, Hokkaido University, Kita 12-jo Nishi 6-chome, Kita-Ku, Sapporo, Hokkaido 060-0812, Japan
[e] Division of Structural Biology, Medical Institute of Bioregulation, Kyushu University, 3-1-1 Maidashi, Higashi-ku, Fukuoka 812-8582, Japan
[f] Department of Pharmacokinetics and Biopharmaceutics, Institute of Biomedical Sciences, Tokushima University, 1-78-1 Shoumachi, Tokushima 770-8505, Japan
[g] Institute of Biomedical Sciences, Academia Sinica, Taipei 11529, Taiwan.
[h] Graduate Institute of Medicine, College of Medicine, Kaohsiung Medical University, Kaohsiung 80708, Taiwan
[i] Department of Molecular Pharmacology, Graduate School of Medicine, Tohoku University, 2-1 Seiryo-machi, Aoba-ku, Sendai, Miyagi 980-8575, Japan
[j] Laboratory for Protein Synthesis and Expression, Institute for Protein Research, Osaka University, 3-2 Yamadaoka, Suita, Osaka 565-0871, Japan
[k] Ph.D. Program in Biomedical Artificial Intelligence, National Tsing Hua University, Hsinchu 300044, Taiwan

ARTICLE INFO

Keywords:
Polyethylene glycol
Anti-PEG antibody
T cell-independent

ABSTRACT

Polyethylene glycol (PEG) is widely used as a standard stealth polymer, although the induction of anti-PEG antibodies and consequent effects have drawn attention in recent years. To date, several anti-PEG antibodies induced by PEG-modified proteins via the T cell-dependent (TD) pathway, in which affinity maturation occurs, have been reported. In contrast, structures of the naïve anti-PEG antibodies before affinity maturation have not been described in the literature. Here, to understand the details of the naïve anti-PEG antibodies capturing PEG, we studied a naïve anti-PEG antibody induced by a PEG-modified liposome in the absence of affinity maturation via the T cell-independent (TI) pathway. The mutation levels, structures as well as in vitro and in silico binding properties of TI and TD anti-PEG antibodies were compared. The TI anti-PEG antibody showed no mutation and a low binding affinity toward PEG, meanwhile, it allowed PEG chain sliding and weak interaction with the terminal group. Furthermore, the naïve anti-PEG antibodies may obtain high affinities by forming tunnel structures via minimal mutations. This research provides new insights into polymer–antibody interactions, which can facilitate the development of novel stealth polymers that can avoid antibody induction.

1. Introduction

Polyethylene glycol (PEG) is a water-soluble polymer with a weakly hydrophobic ethylene and a weakly hydrophilic oxygen as a repeating unit. PEG has no side groups and is highly flexible due to the ether bond in the main chain. Because of these properties, PEG has a low binding affinity toward biomolecules, such as proteins [1]. Therefore, in the past 30 years, PEG has been used as a standard stealth polymer to modify therapeutics such as biomolecules and nanomedicines for enhanced blood retention times and reduced immunogenicity [1]. Nevertheless,

* Corresponding authors.
E-mail addresses: maenaka@pharm.hokudai.ac.jp (K. Maenaka), kakuta@agr.kyushu-u.ac.jp (Y. Kakuta), akitao@life.isct.ac.jp (A. Kitao), mori.takeshi.880@m.kyushu-u.ac.jp (T. Mori).
[1] These authors contributed equally: Yiwei Liu, Takahiro Mori, Yusei Ito and Kimiko Kuroki.
[2] Current affiliation: Department of Chemistry, Graduate School of Science, Nagoya University, Furo-cho, Chikusa-ku, Nagoya, Aichi 464-8602, Japan.

https://doi.org/10.1016/j.jconrel.2025.02.001
Received 31 August 2024; Received in revised form 13 January 2025; Accepted 1 February 2025

accumulating evidence has shown that PEG can also induce the production of antibodies that act against PEG itself [2]. Anti-PEG antibodies lead to accelerated clearance of PEG-modified therapeutics and severe hypersensitive reactions in some cases [2]. Therefore, it is necessary to clarify the mechanism of antibody induction by PEG to develop improved molecular designs and formulations, thus avoiding immune reactions toward stealth polymers.

To gain insight to avoid antibody induction toward PEG, it is necessary to understand the recognition of PEG by naïve B cell receptors (BCRs), which are the causal initial process for the induction of anti-PEG antibodies. Several anti-PEG immunoglobulin G (IgG) clones and their binding complexes with PEG have been revealed through crystallography [3–6], in which some motifs for capture of PEG were clarified. However, all these reported clones were obtained by using PEG-modified proteins that would induce antibodies by T cell-dependent (TD) pathway, in which mutations happened in the variable region of antibodies can raise the affinity toward PEG [2]. The PEG recognition of the mutated antibodies cannot accurately reflect the PEG recognition of the naïve BCRs. PEG-modified therapeutics without protein content, such as liposomes and oligonucleotides, would induce anti-PEG immunoglobulin M (IgM) via the T cell-independent (TI) pathway without affinity maturation. We hypothesized that analysis of those IgMs induced by the TI pathway will unveil the initial PEG recognition by naïve BCRs.

Herein we report the first structural study of an anti-PEG IgM induced by a PEG-modified liposome (PEG-liposome) via the TI pathway. To understand the mechanism by which BCRs on naïve B cells recognize PEG-containing objects, we studied this TI anti-PEG IgM. We also reconstructed the naïve structure of a TD anti-PEG antibody induced by PEG-modified ovalbumin (PEG-OVA) to understand the affinity maturation process. The present work provides insights into each process in the induction of anti-PEG antibodies, which will facilitate the molecular design of stealth polymers that can evade the induction of anti-polymer antibodies.

2. Results

2.1. Anti-PEG IgM

Using the method reported in our previous study [7], we obtained anti-PEG IgM clones M9 and M11 from BALB/c mice, via the immunization of methoxy-PEG2k-liposomes and methoxy-PEG40k-OVA, respectively. M9 and M11 IgMs were expected to be generated from the TI and TD pathways, respectively. Fig. 1 shows the first recognition event between PEG-containing objects and specific BCRs on naïve B cells, in which each component is drawn to reflect its actual molecular size. In the case of the liposome, multiple methoxy-PEG (mPEG) chains on the liposome will be able to crosslink BCRs to induce intracellular signaling for differentiation of the naïve B cell into IgM-producing plasma cells (TI pathway). In contrast, PEG-OVA with a small size may make it difficult to crosslink BCRs. Here naïve B cell requires stimulation by helper T cells to differentiate into plasma cells, which is conducted via recognition of OVA-derived peptide fragments by the helper T cells (TD pathway). Through the process, mutations in the Fv regions of BCR happen to raise the affinity of complementarity-determining regions (CDRs) to PEG.

We reported previously that M9 shows a higher affinity toward methoxy terminal PEG (mPEG) than hydroxy terminal PEG (OH-PEG), whereas M11 shows no difference in affinity toward mPEG and OH-PEG[7]. The DNA sequences of M9 and M11 Fv regions were compared using the V(*D*)J database of BALB/c mice to identify mutations from germline sequences (Fig. 2). In M9, no such mutations were observed as expected. By contrast, mutations were observed in the heavy chain of M11, between CDR2 and CDR3. Within these mutations, four point mutations resulted in three amino acid changes in the linker region and CDR3, and a 6-base insertion resulted in a Val-Ala insertion in HCDR3 (Supplementary Fig. 1a). As a comparison, we analyzed two anti-PEG IgG clones (3.3 and 6.3) [3,4], similarly. These IgG clones were generated from the TD pathway and are highly mutated. Noticeably, an insertion also occurred in the HCDR3 of 6.3 (Supplementary Fig. 1b), which has a similar function to the insertion in the M11 HCDR3 and is critical to raising affinity to PEG (discussed later).

We evaluated the binding of M9 and M11 IgM to PEG using surface plasmon resonance (SPR). M9 and M11 showed concentration-dependent binding responses, and M9 showed weaker responses than M11 (Supplementary Fig. 2). M11 showed similar levels of responses for both OH-PEG and mPEG, while M9 showed higher responses to mPEG than OH-PEG. These results were consistent with our previous report [7], showing that M11 acquired higher affinity against PEG compared with M9 and M9 is more specific to mPEG than OH-PEG; however, binding parameters of both M9 and M11 toward PEGs were difficult to be determined due to the weak response. We further proved the higher affinity of M11 than M9 to PEG by ^{1}H nuclear magnetic resonance (Supplementary Fig. 3).

2.2. Structural analysis of anti-PEG antibodies

To elucidate the PEG recognition mechanism of M9 and M11 antibodies, we prepared crystals using PEG3350 (degree of polymerization, n ~ 76) and determined the crystal structures of Fv-clasp constructs of M9 and M11 in complexes with PEG. We employed Fv-clasp constructs, that is a Fv fragment formed via a coiled-coil domain as a template to enhance the correct paring of heavy and light chains [8]. Supplementary Fig. 4 and Fig. 3 show the overall structures of Fv-clasp complexed with PEG and magnification of PEG recognition sites in each complex, respectively. 12 and 8 repeat units of PEG3350 showed clear electron densities as epitopes in the M9 and M11, respectively.

In the M9-PEG complex, a 12-mer PEG epitope formed a hairpin

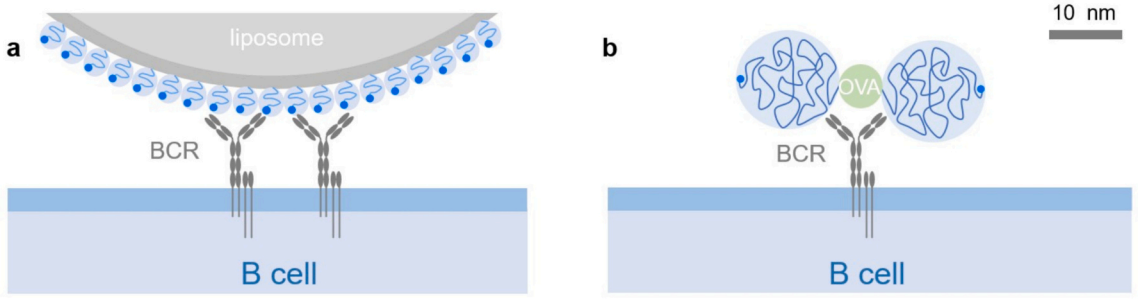

Fig. 1. Illustration of the recognition of PEG-containing objects by specific BCRs on B cells drawn to reflect the molecular size of each component. (a) Recognition of mPEG2k-liposome. BCR, mPEG2k, and liposome are drawn with diameters of ~10 nm, 3.6 nm, and 100 nm, respectively. (b) Recognition of mPEG40k-OVA. mPEG40k and OVA are drawn with diameters of 14 nm and 6 nm, respectively. Blue dots indicate the methoxy terminus of mPEG. Scale bar: 10 nm. (For interpretation of the references to colour in this figure legend, the reader is referred to the web version of this article.)

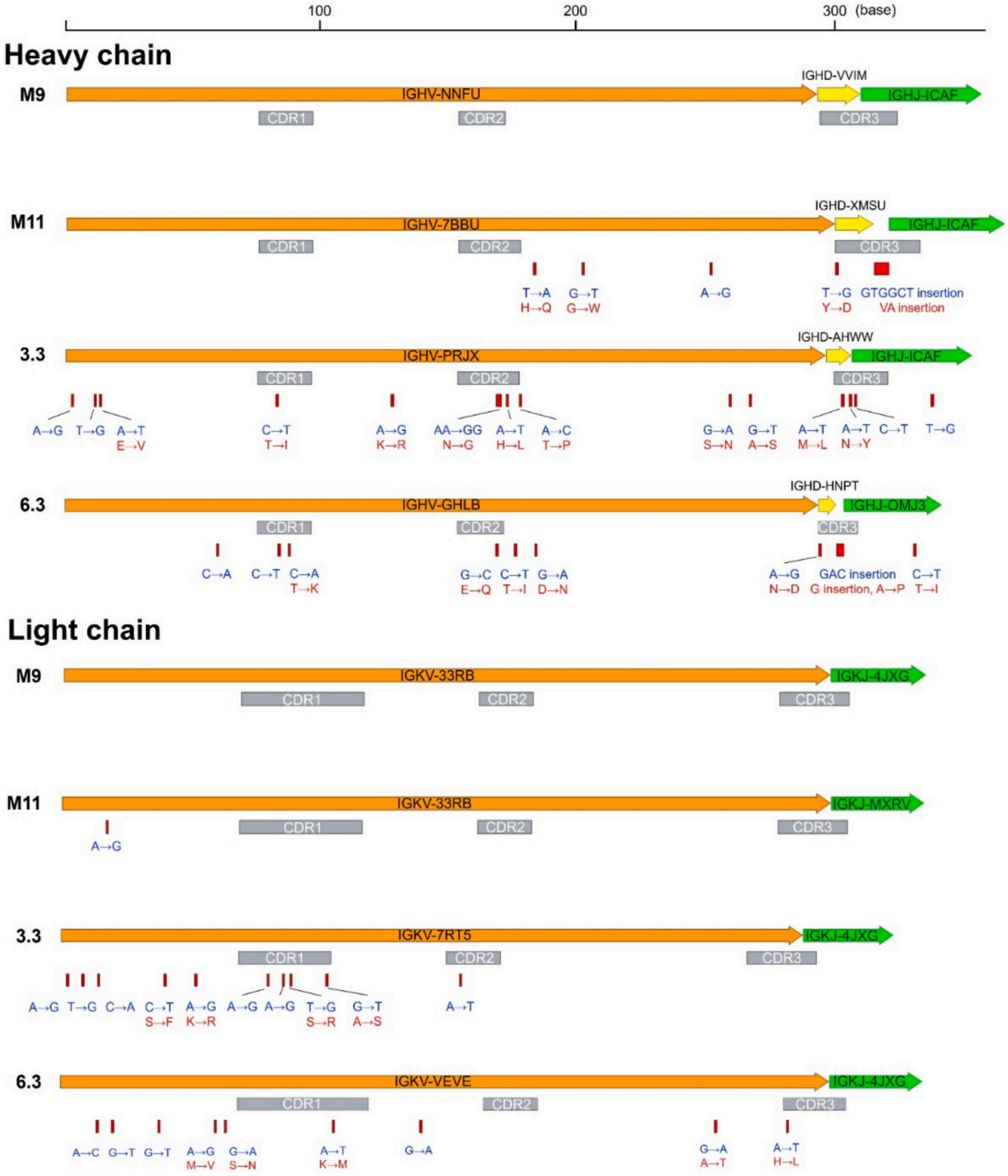

Fig. 2. Identification of V(*D*)J regions and mutations in DNA sequences of anti-PEG antibodies. Results of the heavy chain Fv region and the light chain Fv region, respectively. Blue and red fonts indicate changes in DNA and amino acid sequences, respectively. (For interpretation of the references to colour in this figure legend, the reader is referred to the web version of this article.)

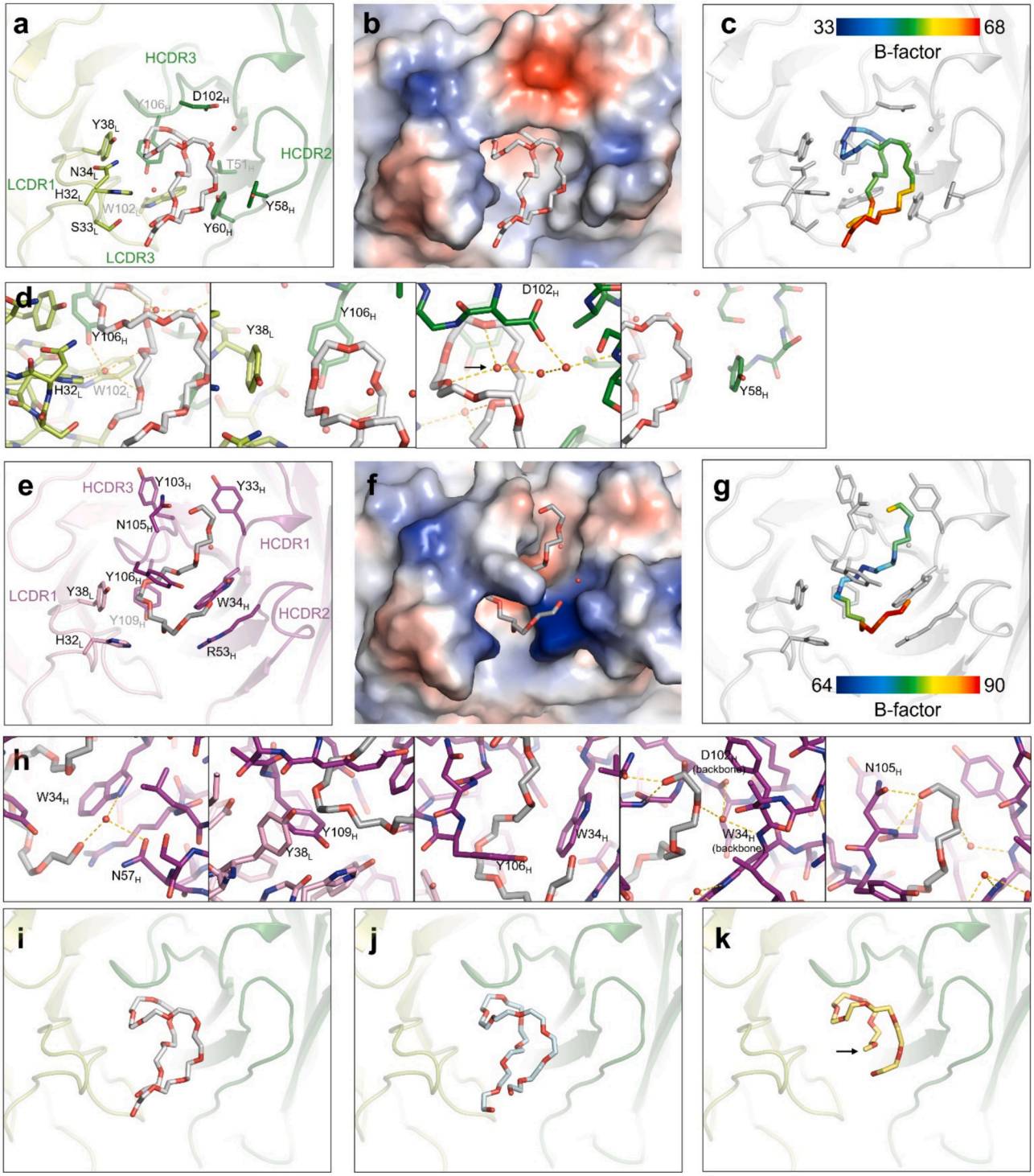

Fig. 3. Structural analysis of complexes of anti-PEG IgM Fv-clasp and PEG. Structure (a, e), electrostatic-potential surface (b, f), and PEG B-factor (c, g) in M9-PEG3350 (a-c) and M11-PEG3350 complex (e-g). Magnified view of interactions of PEG3350 with M9 (d) and M11 (h). Comparison of structures of M9 with PEG3350 (i), PEG2000 MME (j), and PEG550 DME (k). The arrow in k points to the methoxy terminus of PEG550 DME.

structure and was embedded into a pocket surrounded by HCDR2, HCDR3, LCDR1, and LCDR3 (Fig. 3a, b). In the M11-PEG complex, an 8-mer PEG epitope passed through a groove (Fig. 3e, f). Above the groove, $Y106_H$ in HCDR3 and $W34_H$ in HCDR1 formed a tunnel with a diameter of approximately 6.8–8.8 Å, which prevents the release of PEG chains. This structural feature was interpreted as critical to the high PEG binding affinity of M11. Val-Ala was found to be inserted just before the $Y106_H$ during affinity maturation (Supplementary Fig. 1a). To understand the effect of the insertion, the predicted structures of the naïve M11 single chain Fv (scFv) fragment, in which mutations were returned to the original sequences were generated by AlphaFold2. The naïve M11 shows a groove similar to that in the M11 paratope but the tunnel of Y—W above the groove disappeared for the original position of Y (Supplementary Fig. 5). This result indicates that Val-Ala insertion shifted the $Y106_H$ position, which allowed the formation of the tunnel structure. Comparably, clone 6.3 has been reported to have a tunnel

structure to capture PEG chains similar to that in M11 [4]. A similar insertion of Gly just before a Y—W tunnel structure was found in the heavy chain of clone 6.3 (Fig. 2, Supplementary Fig. 1b), which seems to be critical for tunnel formation. Thus, insertion of one or two amino residues would be a common mutation to capture PEG chains via tunnel formation.

The mode of molecular interactions of M9 and M11 with PEG was compared. In the M9-PEG recognition, B-factor values of the hairpin loop of PEG are low, indicating the restricted mobility of this region by the tight recognition of M9 (Fig. 3c). The loop is recognized via water-mediated hydrogen bonding with $D102_H$ and hydrophobic interactions with $Y38_L$ and $Y106_H$ (Fig. 3d). One water molecule was bound to the center of the loop of the bound PEG (pointed by arrow in Fig. 3d), which stabilized the loop structure. M9 utilizes water molecules effectively to recognize the PEG chain. In contrast, in the M11-PEG recognition, water molecules are excluded from the interface. The center of the bound PEG chain that passes through the tunnel structure has low B-factor values (Fig. 3g). This region is recognized by multiple hydrophobic interactions

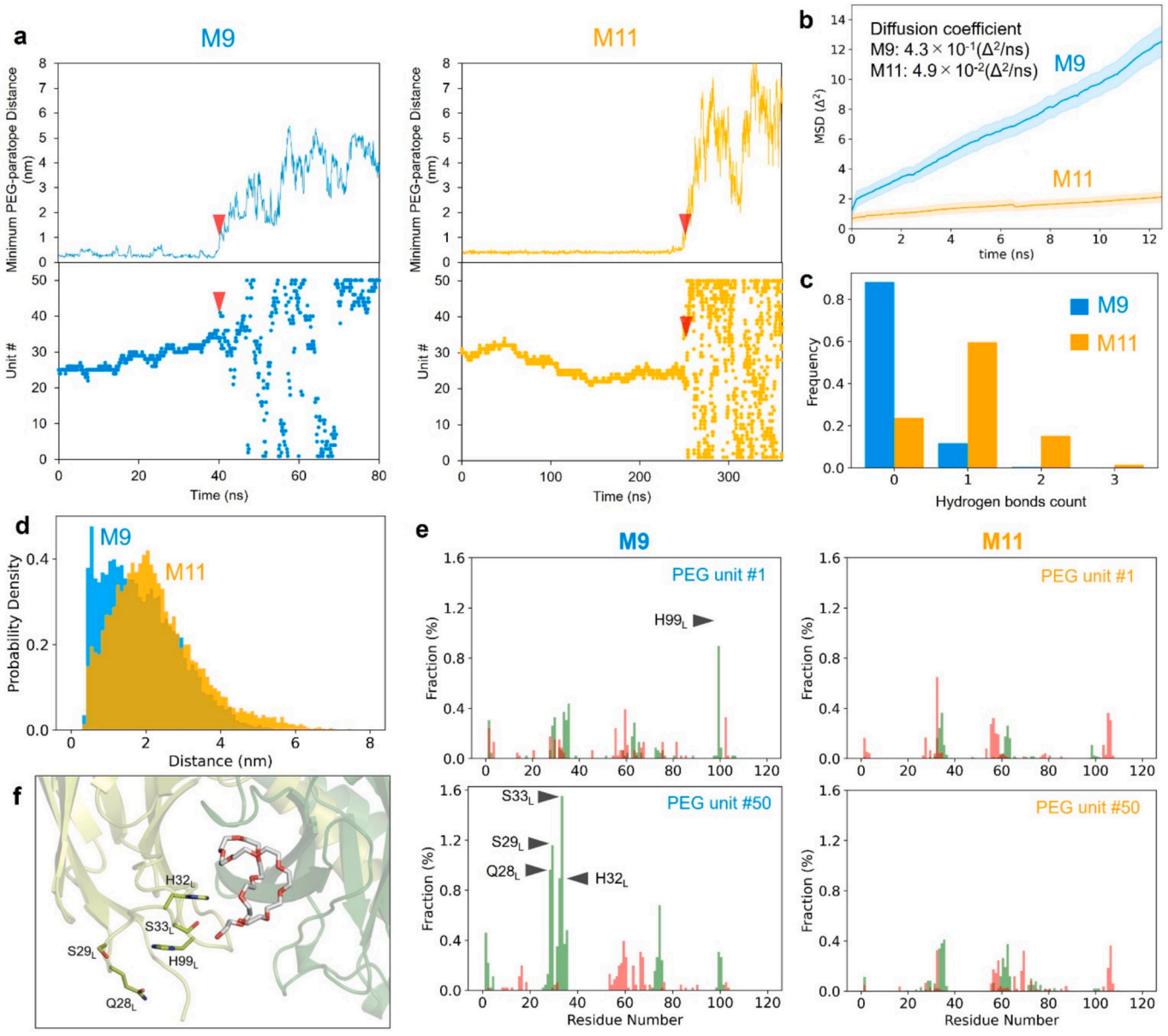

Fig. 4. Interactions between Fv-clasp and PEG. (a) Minimum PEG–paratope distance defined as the minimum inter-center of mass distance between the paratope and the closest PEG unit (upper graph) and PEG unit number closest to the paratope (lower graph) during representative MD simulations for M9 (left) and M11 (right). The center of mass of the paratopes is defined as the center of mass of S98–W102 (the light chain) and Y101–Y105 (the heavy chain) of M9 and that of S98–W102 (the light chain) and R101–N105 (the heavy chain) of M11. Red triangles indicate when Fv-claps/PEG complexes are dissociated. (b) Mean square displacements (MSD) of PEG sliding shown by the nearest PEG unit numbers closest to the paratope of M9 and M11 as a function of time. Δ represents a shift of PEG unit number caused by PEG sliding. Lines and shades represent averages and standard errors, respectively. (c) Numbers of direct hydrogen bonds between PEG and the paratope of M9 and M11. (d) Distributions of the minimum distance between the PEG terminus (PEG unit #1 or #50) and the Fv-clasp of M9 and M11 indicated by probability density. (e) Contact probabilities between residues in Fv-clasp and the PEG terminus (PEG unit #1 or #50) shown by fraction of contacted time (%). Contacts were made if the minimum inter-heavy atom distance between the pairs was ≤0.5 nm. Top 5 amino acid residues in M9 are marked. Red and green bars show residues in heavy and light chains, respectively. Fractions were calculated within the period of PEG binding with paratope in respective simulations. (d) to (f) are from the sum of six simulations for each complex. (f) Top five amino acid residues of M9 in panel e are marked in crystal structure. (For interpretation of the references to colour in this figure legend, the reader is referred to the web version of this article.)

with $W34_H$, $Y106_H$, $Y109_H$, and $Y38_L$, where water molecules are excluded (Fig. 3h). Both crystals of M9 and M11 complexed with PEG included two molecules in a unit cell. Features of PEG recognitions mentioned above for M9 and M11 were consistent for the two molecules (Supplementary Fig. 6).

To understand the structural features needed for terminal methoxy group recognition by M9, we compared the crystal structures of M9 in complexes with short PEG550 DME (methoxy group at both termini, n ~ 13) and PEG2000 MME (methoxy group at one terminus, n ~ 45) with PEG3350 (hydroxy group at both termini, n ~ 76). All three complexes shared a similar paratope structure in M9 and epitope shape in PEG chains (Fig. 3i-k). Of note, one terminal methoxy group was located within the paratope in the complex with a very short PEG550 DME (Fig. 3k, Supplementary Fig. 7). Such a location of the methoxy terminal within the paratope was not observed in the complex with longer PEG2000 MME although it has methoxy terminus (Fig. 3j). These results indicates that the terminal methoxy group recognition by the paratope observed in PEG550 DME is not strong.

2.3. Molecular dynamics (MD) simulations of anti-PEG antibodies

To investigate the effects of the terminal group of PEG on the binding of PEG to anti-PEG IgM in detail, MD simulations of the binding of PEG to Fv-clasp constructs were carried out. The simulations were set up using the crystal structures of M9 and M11 Fv-clasp constructs. PEG 2 k ($n = 50$) was set up on the original PEG epitope at the center of the PEG chain, and independent MD simulations were conducted 6 times for each clone (Supplementary videos 1–12). PEG was bound to the paratope with a close distance of approximately 5 Å until it was released after a certain time (Fig. 4a upper panel, and Supplementary Fig. 8). M9 had a shorter epitope–paratope binding duration than M11 (less than 100 ns in 4 of 6 simulation results), which was consistent with its lower affinity toward PEG. Interestingly, PEG was bound to the paratope while the binding site within the PEG chain changed continuously (Fig. 4a lower panel, and Supplementary Fig. 8), showing the sliding of PEG chain within the paratope. Particularly, PEG sliding in M9 continued until the binding region approached the position close to the PEG terminus, after which point the PEG was released (Fig. 4a, Supplementary Fig. 8a). PEG sliding was 8.8-fold faster in M9 than in M11 (Fig. 4b), reflecting the lower affinity of M9 than that of M11.

The direct interaction of PEG with Fv-clasp was evaluated by the frequency of direct hydrogen bond formation (Fig. 4c). During binding with PEG, the frequency of direct hydrogen bond formation of M9 with the PEG chain was smaller than that of M11, which indicated more possibility of direct interaction with PEG in M11, consistent with the structural properties showed in crystal structures (Fig. 3d, h).

Concerning the recognition of the terminal methoxy group of PEG in M9, we found that the average distance of M9 with the termini of PEG (unit #1 and #50) was smaller than that of M11 (Fig. 4d), reflecting the higher frequency of the interactions between PEG terminus and the amino acid residues in M9 than in M11. We picked up the possible amino acid residues that bind with the PEG terminus with a distance of closer than 5 Å (Fig. 4e). In M9, the top 5 amino acid residues with high fractions ($H99_L$ for PEG unit #1, and $Q28_L$, $S29_L$, $H32_L$, and $S33_L$ for PEG unit #50) were highlighted as the possible binding sites of PEG terminus (Fig. 4f). In the crystal structure, those amino acid residues are located on CDR1 and CDR3 of the light chain near the PEG epitope, where PEG terminal methoxy group is present (Fig. 4f). Hydrogen bond formation between the PEG terminal methoxy group and those amino acid residues was confirmed in the simulations (Supplementary videos 1–12 and Supplementary Fig. 9). Comparatively, the terminus binding events in M11 occupied a lower fraction than in M9 (Fig. 4e).

3. Discussion

3.1. Recognition mechanisms of two anti-PEG antibodies

M9 is the first reported crystal structure of an anti-PEG antibody induced by the TI pathway which maintains the naïve BCR sequence. According to the elucidated crystal structure of the complex, PEG in a hairpin loop conformation was embedded in a pocket structure of M9. Similar loop conformations were also observed in TD anti-PEG antibody clones (3.3, 2B5, 6.3, h15-2b) previous reported [3–5]. Unlike those TD anti-PEG antibodies, lack of direct hydrogen bonding with paratope lead to a low binding affinity between PEG and M9. In the case of M11, which was induced by the TD pathway, a linear PEG chain was trapped in a groove with a tunnel structure. Similar to M11, clone 6.3 also has a tunnel structure with a diameter of approximately 6.8–8 Å, which is critical for holding PEG chains with high affinity [4]. The tunnel structure can capture the PEG chain directly via hydrophobic interaction.

MD simulations of PEG antibodies are reported here for the first time. We found that flexible PEG slid through the paratope via the dynamic exchange of bound monomeric units. The sliding was much faster in M9 than in M11, reflecting the weaker binding affinity of PEG toward M9 than toward M11. M9 released the PEG chain when PEG slid and reached approximately the last 10 monomeric units (simulation 1, 2, 4, and 5 in Supplementary Fig. 8a). This is close to the length of the epitope of the PEG chain shown in the crystal structure of M9, which is possibly the minimum size for stable binding. The allowance of sliding extended the binding duration of PEG with M9, resulting in the reduction of the off-rate (k_{off}) of binding. The enhancement of binding time should be important in BCR activation, especially for the naïve BCR activation by PEG binding [9].

Recognition of the methoxy terminal by M9 is different from the mPEG-specific clone h15-2b, induced by the TD pathway. Clone h15-2b has a specific hydrophobic pocket for binding with the methoxy terminal group into which the PEG chain is vertically inserted[5]. By contrast, M9 showed interactions with the terminal methoxy group at light chain CDR nearby the paratope, via a cluster of hydrogen bond-forming amino acid residues (Fig. 4e and Fig. 4f). Compared to a terminal hydroxy group, the somewhat lower solubility of the terminal methoxy group may enhance the formation of hydrogen bonding with M9 rather than free water, which explains the higher affinity of M9 to mPEG than OH-PEG. It should be noted that these interactions were transient, which occupied a limited time fraction in the whole time of PEG-paratope binding. As a result, PEG terminal methoxy group binding at that region cannot be identified in the crystal structure of the M9-PEG complex. Although terminus binding events are also observed in M11, the fraction of the events was smaller than those with M9 (Fig. 4e). This is the reason why M11 does not show binding specificity to PEG terminal group.

3.2. Process of IgM induction by TI and TD-antigens

Anti-PEG IgM clone M9 with a low affinity toward PEG was induced via the TI pathway without affinity maturation, which was confirmed by comparing its DNA sequence with germline gene sequences (Fig. 2). We consider the process of IgM induction of M9 by PEG-liposomes as follows (Fig. 1a). PEG-liposomes can crosslink the BCRs on a specific B cell clone to induce intracellular signaling for differentiation into a plasma cell without affinity maturation, which then produces anti-PEG IgM. The diameter of the PEG-liposome is approximately 100 nm, and its surface is closely filled with mPEG2k chains (assuming the PEG diameter of 3.6 nm) [10]. Because PEG-liposome is significantly larger than BCRs (~10 nm) in size, PEG-liposome can be bound to BCR with significantly high avidity (multiple PEG chains are assignable to one BCR). Thus, PEG-liposome can be bound to BCR with sufficient affinity to induce signaling even though 1:1 binding affinity is quite small (Supplementary Fig. 2, 3). According to the determined crystal structure and MD

simulations, M9 recognizes PEG by intrinsically weak interactions: indirect hydrogen bonding mediated by water molecules, sliding of PEG for extension of binding duration as well as dynamic interactions with methoxy terminal groups. To evade antibody induction, polymers can be designed with side groups in a random manner that are less susceptible to sliding on BCRs. Another possible design is a polymer with weak hydration, which destabilizes water-mediated indirect hydrogen bonding with BCRs [11]. Some zwitterionic polymers do not induce the production of antibodies, which is attributed to their weak hydration [12,13].

We also consider the process of IgM induction by mPEG40k-OVA conjugate via the TD pathway as follows (Fig. 1b). Because the size of PEG-OVA, which has at most two PEG chains on one OVA, is comparable to that of BCR, the crosslinking of BCRs will be difficult. Meanwhile, once the PEG chain of PEG-OVA is captured by the naïve BCR, PEG-OVA can be endocytosed to start the affinity maturation process. Here OVA-derived peptides are used as T-cell epitopes to proceed the TD pathway. Before affinity maturation, naïve BCR may bind the PEG chain weakly by grooves, like the predicted structures of naïve M11 shown in Supplementary Fig. 5. The critical mutation required to raise the affinity of BCRs toward the PEG chain is the insertion of amino acids (Val-Ala in M11), which allows the formation of a tunnel to capture a single PEG chain, leading to direct contact with the PEG chain via the hydrophobic interactions. We found that a similar tunnel structure reported for clone 6.3 was also induced by a similar insertion (Fig. 2 and Supplementary Fig. 1). Thus, the insertion-triggered tunnel formation may be a general strategy of B cells to capture the PEG chain with high affinity via a small number of mutations. To avoid recognition of a polymer chain by the tunnel structures, introducing side groups on the polymer chain for chain thickening may be an effective design.

3.3. Limitations of this study

This research focused on investigating two anti-PEG IgM clones, M9 and M11, as representatives for anti-PEG antibodies generated through TI and TD pathways, respectively. It should be acknowledged that the sample size of anti-PEG antibodies analyzed is limited, particularly for those with detailed gene and structural information. Although some common properties of anti-PEG antibodies were suggested by comparing our results with previous studies, the diversity and complexity of the polyclonal anti-PEG antibody response remain unclear. Further studies are required to clarify the mechanisms underlying polyclonal anti-PEG antibody generation in response to PEGylated drugs and daily-life exposure to PEG-containing materials. Regarding the evaluation of binding affinity, the relatively weak interaction of M9 with PEG presented challenges in determining the affinity by SPR method. Alternative approaches or enhanced methodologies are required to accurately measure the affinity of those naïve anti-PEG antibody clones. In the simulation study, we utilized a simplified model as an initial approach. This model did not account for more complex scenarios, such as tethered PEG chains or multivalent interactions, which may better reflect real interactions between PEG and BCRs or antibodies. Incorporating these factors into future simulations will provide a more comprehensive understanding of these interactions.

4. Conclusions

Here we reveal strategies used by naïve BCRs to capture PEG chains. First, BCRs recognize a flexible PEG chain as a sequence of monomeric units. Second, BCRs allow the sliding of the PEG chain with the same repeating monomeric unit to extend the binding duration. Third, a PEG chain without side groups can be captured by a narrow tunnel-like structure which is acquired by a small number of mutations of naïve BCRs. Fourth, the PEG terminus, which occupies an extremely small portion of the PEG chain, has a significant effect on raising the affinity via weak interactions nearby the paratope. These points may commonly exist in naïve BCRs capturing other flexible hydrophilic polymers and should be considered in the design of novel stealth polymers that can evade antibody induction.

5. Materials and methods

The detailed materials and methods can be found in the Supplementary Information.

Supplementary data to this article can be found online at https://doi.org/10.1016/j.jconrel.2025.02.001.

CRediT authorship contribution statement

Yiwei Liu: Writing – review & editing, Writing – original draft, Visualization, Investigation. **Takahiro Mori:** Writing – review & editing, Visualization, Investigation. **Yusei Ito:** Writing – review & editing, Visualization, Software, Investigation. **Kimiko Kuroki:** Writing – review & editing, Visualization, Investigation. **Seiichiro Hayashi:** Writing – review & editing, Visualization, Investigation. **Daisuke Kohda:** Writing – review & editing, Visualization, Investigation. **Taro Shimizu:** Writing – review & editing, Resources. **Tatsuhiro Ishida:** Writing – review & editing, Resources, Funding acquisition. **Steve R. Roffler:** Writing – review & editing, Investigation. **Mika K. Kaneko:** Writing – review & editing, Investigation. **Yukinari Kato:** Writing – review & editing, Investigation, Funding acquisition. **Takao Arimori:** Writing – review & editing, Methodology. **Takamasa Teramoto:** Writing – review & editing, Visualization, Investigation. **Kazuhiro Takemura:** Writing – review & editing, Visualization, Software, Investigation. **Kenta Ishibashi:** Writing – review & editing, Investigation. **Yoshiki Katayama:** Writing – review & editing, Funding acquisition. **Katsumi Maenaka:** Writing – review & editing, Supervision, Funding acquisition, Conceptualization. **Yoshimitsu Kakuta:** Writing – review & editing, Supervision, Funding acquisition, Conceptualization. **Akio Kitao:** Writing – review & editing, Supervision, Funding acquisition, Conceptualization. **Takeshi Mori:** Writing – review & editing, Writing – original draft, Supervision, Project administration, Funding acquisition, Conceptualization.

Declaration of competing interest

There are no conflicts to declare.

Acknowledgements

We thank Prof. Daron M. Standley (Osaka University) and Prof. Koichi Shiraishi (The Jikei University School of Medicine) for critical reading and advising of the manuscript. This work was supported by Grant-in-Aid for Transformative Research Areas (A) (20H05876), awarded to Takeshi Mori, by Japanese Science and Technology Agency (JST) Support for Pioneering Research Initiated by the Next Generation (SPRING) under Grant Number JPMJSP2136, awarded to Takahiro Mori, and by Grant-in-Aid for Scientific Research (B) (23H03739), awarded to Tatsuhiro Ishida. The sequencing of M9 and M11 was supported in part by the Japan Agency for Medical Research and Development (AMED) under Grant Number JP22ama121008, awarded to Yukinari Kato. The MD simulation was supported by MEXT/JSPS KAKENHI Nos. JP23H04058, JP21H05510, JP22H04745, and JP19H03191, awarded to Akio Kitao, and by MEXT as a "Program for Promoting Researches on the Supercomputer Fugaku" (Application of Molecular Dynamics Simulation to Precision Medicine Using Big Data Integration System for Drug Discovery, JPMXP1020200201 and Biomolecular Dynamics in a Living Cell, JPMXP1020200101), awarded to Akio Kitao. MD simulations used computational resources of the supercomputer TSUBAME provided by the Tokyo Institute of Technology, FUGAKU through the HPCI System Research Project (Project IDs: hp220164, and hp220170), Research Center for Computational Science, The National Institute of Natural Science (Project: 22-IMS-C051), and

The Institute for Solid State Physics, The University of Tokyo (Project: 2022-Ca-0025).

Data availability

The data supporting this article have been included as part of the Supplementary Information. Crystallographic data for M9-PEG3350, M9-PEG2000 MME, M9-PEG550 DME and M11-PEG3350 has been deposited at the PBD under 8IQP, 8IQQ, 8IQR and 8IQS.

References

[1] F.M. Veronese, G. Pasut, PEGylation, successful approach to drug delivery, Drug Des. Discov. 10 (2005) 1451–1458, https://doi.org/10.1016/S1359-6446(05)03575-0.

[2] B.M. Chen, T.L. Cheng, S.R. Roffler, Polyethylene glycol immunogenicity: theoretical, clinical, and practical aspects of anti-polyethylene glycol antibodies, ACS Nano 15 (2021) 14022–14048, https://doi.org/10.1021/acsnano.1c05922.

[3] C.C. Lee, Y.C. Su, T.P. Ko, L.L. Lin, C.Y. Yang, S.S.C. Chang, S.R. Roffler, A.H. J. Wang, Structural basis of polyethylene glycol recognition by antibody, J. Biomed. Sci. 27 (2020) 1–13, https://doi.org/10.1186/s12929-019-0589-7.

[4] J.T. Huckaby, T.M. Jacobs, Z. Li, R.J. Perna, A. Wang, N.I. Nicely, S.K. Lai, Structure of an anti-PEG antibody reveals an open ring that captures highly flexible PEG polymers, Commun. Chem. 3 (2020) 124, https://doi.org/10.1038/s42004-020-00369-y.

[5] M.T.T. Nguyen, Y.C. Shih, M.H. Lin, S.R. Roffler, C.Y. Hsiao, T.L. Cheng, W.W. Lin, E.C. Lin, Y.J. Jong, C.Y. Chang, Y.C. Su, Structural determination of an antibody that specifically recognizes polyethylene glycol with a terminal methoxy group, Commun. Chem. 5 (2022) 88, https://doi.org/10.1038/s42004-022-00709-0.

[6] C.Y. Hsiao, J.L. Meng, J.Z. Hong, X.H. Ly, M.H. Lin, C.Y. Chang, M.T.T. Nguyen, T. L. Cheng, W.W. Lin, P.A. Burnouf, T.S. Al-Qaisi, E.S. Liu, Y.C. Su, Engineering a high-affinity anti-Methoxy poly (ethylene glycol)(mPEG) antibody for sensitive Immunosensing of mPEGylated therapeutics and mPEG molecules, Bioconjug. Chem. 33 (2022) 2180–2188, https://doi.org/10.1021/acs.bioconjchem.2c00416.

[7] Y. Hashimoto, T. Shimizu, Y. Mima, A.S.A. Lila, T. Ishida, H. Kiwada, Generation, characterization and in vivo biological activity of two distinct monoclonal anti-PEG IgMs, Toxicol. Appl. Pharmacol. 277 (2014) 30–38, https://doi.org/10.1016/j.taap.2014.03.002.

[8] T. Arimori, Y. Kitago, M. Umitsu, Y. Fujii, R. Asaki, K. Tamura-Kawakami, J. Takagi, Fv-clasp: an artificially designed small antibody fragment with improved production compatibility, stability, and crystallizability, Structure 25 (2017) 1611–1622, https://doi.org/10.1016/j.str.2017.08.011.

[9] J. Corzo, Time, the forgotten dimension of ligand binding teaching, Biochem. Mol. Biol. Educ. 34 (2006) 413–416, https://doi.org/10.1002/bmb.2006.494034062678.

[10] A.K. Kenworthy, K. Hristova, D. Needham, T.J. McIntosh, Range and magnitude of the steric pressure between bilayers containing phospholipids with covalently attached poly (ethylene glycol), Biophys. J. 68 (1995) 1921–1936, https://doi.org/10.1016/S0006-3495(95)80369-3.

[11] Q. Shao, S. Jiang, Influence of charged groups on the properties of zwitterionic moieties: a molecular simulation study, J. Phys. Chem. B 118 (2014) 7630–7637, https://doi.org/10.1021/jp5027114.

[12] B. Li, Z. Yuan, H.C. Hung, J. Ma, P. Jain, C. Tsao, J. Xie, P. Zhang, X. Lin, K. Wu, S. Jiang, Revealing the immunogenic risk of polymers, Angew. Chem. Int. Ed. 57 (2018) 13873–13876, https://doi.org/10.1002/anie.201808615.

[13] B. Li, P. Jain, J. Ma, J.K. Smith, Z. Yuan, H.C. Hung, Y. He, X. Lin, K. Wu, J. Pfaendtner, S. Jiang, Trimethylamine N-oxide–derived zwitterionic polymers: a new class of ultralow fouling bioinspired materials, Sci. Adv. 5 (2019) eaaw9562, https://doi.org/10.1126/sciadv.aaw9562.